Metal-Free Catalysis

DOI: 10.1002/anie.201404333

High-Rate Oxygen Electroreduction over Graphitic-N Species Exposed on 3D Hierarchically Porous Nitrogen-Doped Carbons**

*Wenhui He, Chunhuan Jiang, Jiabo Wang, and Lehui Lu**

Abstract: *Nitrogen-doped species (NDs) are theoretically accepted as a determinant of the catalytic activity of metal-free N-doped carbon (NC) catalysts for oxygen reduction reaction (ORR). However, direct relationships between ND type and ORR activity have been difficult to extract because the complexity of carbon matrix impairs efforts to expose specific NDs. Herein, we demonstrate the fabrication of a 3D hierarchically porous NC catalyst with micro-, meso-, and macroporosity in one structure, in which sufficient exposure and availability of inner-pore catalytic sites can be achieved due to its super-high surface area (2191 $cm^2 g^{-1}$) and interconnected pore system. More importantly, in-situ formation of graphitic-N species (GNs) on the surface of NC stimulated by KOH activation enables us to experimentally reveal the catalytic nature of GNs for ORR, which is of great significance for the design and development of advanced metal-free NC electrocatalysts.*

Developing highly active and cost-effective catalysts for the oxygen reduction reaction (ORR) is paramount to achieving a large-scale commercialization of fuel cells.[1] In this regard, metal-free nitrogen-doped carbon (NC) materials as alternative to platinum-based catalysts for ORR have become an active field of research in recent years, owing to their low cost, environmental friendliness, high electrocatalytic selectivity and good durability.[2] According to experimental studies[3] and theoretical calculations,[4] the observed catalytic activity of metal-free NC materials toward ORR originates from the doping effect of N atoms, which disrupt the electroneutrality of adjacent C atoms and create positively charged sites favorable for O_2 adsorption and reduction. Among three types of theoretically active N-doped species (NDs), pyridinic and pyrrolic N are always located on the graphite edge, while quaternary N can be both "edge-valley-N" ($N\text{-}Q_{valley}$) and "bulk-like-N" (also known as graphitic-N species, GNs).[3a] Even with a high level of research activity, however, the nature of catalytic sites in the metal-free NC catalysts, especially relationships between ND type and ORR activity, has been heavily debated,[3] because of two main technical barriers: 1) depending on synthesis conditions, N doping level and the type of NDs in NC can vary significantly;[3a,b,5] 2) an inevitable tendency of all NC nanostructures during the thermal annealing and/or the removal of templates is the incidental sintering and re-stacking,[6] leading to the embedment of a large fraction of NDs into the graphitic matrix. Yet, understanding the correlation between specific NDs and ORR activity is a necessary step toward rational design and construction of advanced metal-free NC catalysts.

To maximize the number of exposed-edge NDs, previous studies have been focused on N-doped graphene,[3a,6] carbon nanotubes,[3b,7] and nanofiber.[8] In this context, $N\text{-}Q_{valley}$ species are proved to be highly active sites to catalyze ORR through a four-electron process.[3a–d] Nonetheless, GNs, also as a quaternary N, exhibit a controversial ORR catalytic activity,[3d,e,6] because they are confined within the carbon lattice and tend to be spontaneously buried into the carbon matrix. In principle, different from pyridinic N species, GNs are not bonded to metal cation through forming coordination complexes so that their catalytic activity is not affected by the controversial role of metallic impurities,[9] which helps to identify the nature of the nitrogen atoms in metal-free NC catalysts. On the other hand, the catalytic properties of metal-free NC materials are severely influenced by the porosity of the carbon matrix which is critical for mass transport of ORR-related agents.[2d] Incorporation of large pores into meso-/microporous structures has been utilized for preparing a variety of hierarchically porous carbons with low mass transfer resistance,[10] but none of these studies reported to date could effectively mitigate the embedment effects of GNs. Hence, it remains a great challenge to identify a suitable strategy to enhance the exposure of special NDs while optimizing the three-dimensional (3D) structure of carbon matrix for mitigating the effect from the structure-dependent mass-diffusion limitations.

Herein, we present a novel and general strategy referred to as "mussel-inspired surface chemistry" for the construction of 3D hierarchically porous NC catalysts with a super-high surface area (2191 $cm^2 g^{-1}$) by using polydopamine (PDA)-modified mixed cellulose ester filter films (MCEFs) as a sole template. The multifunctionality of PDA-modified MCEFs (p-MCEFs) and the assistance of KOH activation seem to be the key to obtaining a hierarchically porous NC material with exposed GNs on the surface layer, which helps to screen the effect of structure on the ORR-catalytic activity and to further reveal the catalytic nature of GNs. Our experimental results showed that when GNs were in-situ generated on the

[*] W. H. He, C. H. Jiang, Prof. L. H. Lu
State Key Laboratory of Electroanalytical Chemistry, Changchun Institute of Applied Chemistry, Chinese Academy of Sciences
5625 Renmin Street, Changchun 130022 (P.R. China)
E-mail: lehuilu@ciac.ac.cn
J. B. Wang
Chemistry and Life Science School
Changchun University of Technology
Changchun, 130022 (P.R. China)

[**] Financial support by the NSFC (No. 21125521) and the National Basic Research Program of China (973 Program, No. 2010CB933600) is gratefully acknowledged.

Supporting information for this article is available on the WWW under http://dx.doi.org/10.1002/anie.201404333.

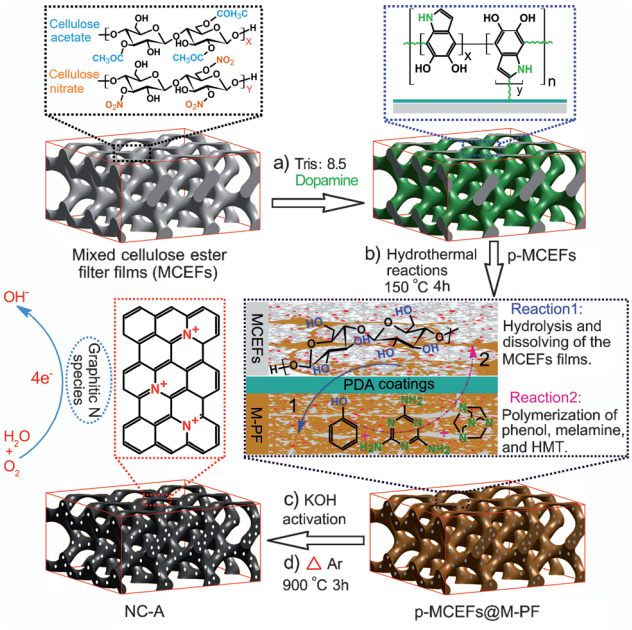

Figure 1. Fabrication and formation mechanism of the 3D hierarchically porous nitrogen-doped carbon materials. Tris = tris buffer solution (pH 8.5); HMT = hexamethylenetetramine.

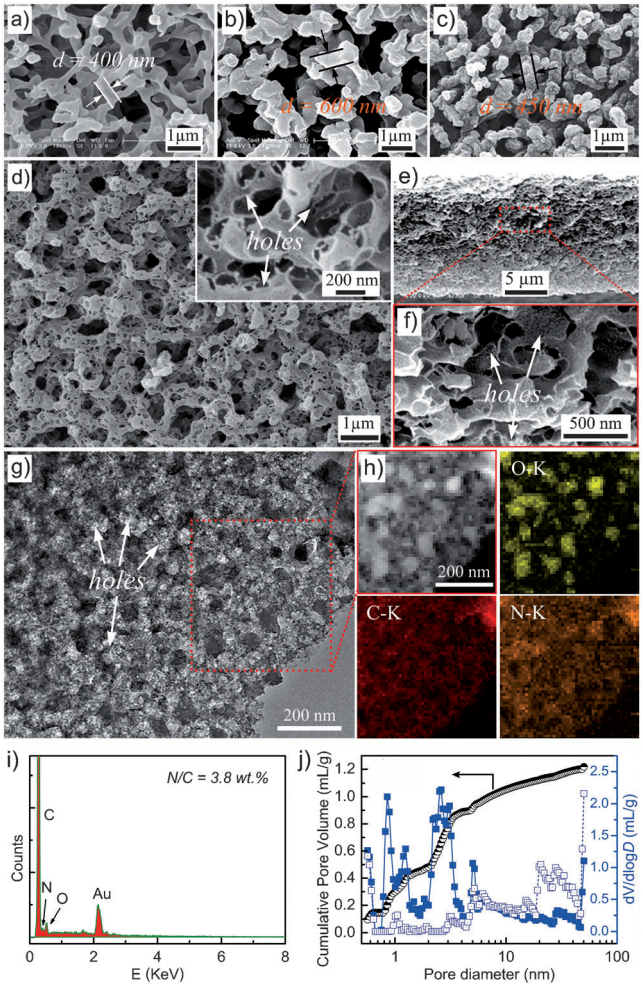

Figure 2. SEM images of a) MCEFs films, b) p-MCEFs@M-PF resins, c) NC-U, and d) NC-A carbon materials. Inset in (d) shows a magnified SEM image of NC-A. e,f) Cross-sectional SEM images of NC-A. g) TEM image, h) high-angle annular dark-field scanning TEM image and corresponding EDX elemental mapping images of NC-A. i) EDX energy spectrum of NC-A. j) Cumulative pore volume of NC-A (black circles) and pore size distribution of NC-A (blue solid squares) and NC-U (blue hollow squares).

surface of NC, ORR on the as-prepared NC catalysts was greatly promoted and proceeded through a four-electron process in basic solutions, clarifying the pivotal role played by GNs in the catalytic process.

The synthesis of 3D hierarchically porous NC materials is illustrated in Figure 1. Commercial MCEFs with macroporous frameworks (Figure 2a and Supporting Information Figure S1) and varying pore sizes (0.2–1.2 μm, 0.6 μm chosen here) were used as the template for the sequential modification of PDA and melamine-doped phenol formaldehyde (M-PF) resins. The PDA coatings,[11] as adherent layers, enabled the preferential formation of M-PF resins on the surface of p-MCEFs. A representative scanning electron microscopy (SEM) image reveals that the p-MCEFs surfaces are uniformly covered by M-PF resins (p-MCEFs@M-PF), accompanied by a notable increase of skeleton diameter (Figure 2b and S2a–d). The successful incorporation of melamine into the M-PF resins was confirmed by the characteristic absorption of melamine derivatives in the FT-IR spectra (Figure S3) and by the recorded N doping in X-ray photoelectron spectrometry (XPS) and elemental analysis (EA) (Figure S4). Direct annealing of the p-MCEFs@M-PF in Ar led to the formation of NC films with 3D macroporous frameworks (hereafter designated as NC-U) (Figure 2c and S2e–h). Taking into account the low thermal stability and neglectable carbon yield of MCEFs in Ar (Figure S5a), the NC-U should be mainly derived from the carbonization of M-PF resins (about 35% carbon yield at 900 °C, Figure S5a). Meanwhile, the p-MCEFs may serve as pore-generating agents in view of numerous holes formed in the skeleton of NC-U (Figure S2h). However, the NC-U only showed a moderate Brunauer–Emmet–Teller (BET) surface area (S_{BET}) of 696.4 $cm^2 g^{-1}$, with an average pore size of 11 nm (see Figure S6 for N_2 sorption measurements). Given the potential of high S_{BET} to enhance the exposure of NDs, we tried to increase the S_{BET} of NC by activating p-MCEFs@M-PF resins with KOH.[12] In this process, the melamine molecules incorporated into M-PF resins were preserved (Figure S3), and more importantly, the corresponding NC films formed under KOH-assisted annealing (hereafter denoted as NC-A) showed abundant holes on the wall of their well-maintained 3D bi-continuous frameworks (Figure 2d–f and S7a,b).

Figure 2g shows a representative transmission electron microscopy (TEM) image of NC-A, displaying two types of carbon morphologies: carbon nanoparticles and sponge-like carbon films. On the basis of energy-dispersive X-ray (EDX) elemental mapping images showing an obviously different distribution of O atoms in these two morphologies (Figure 2h), we assumed that the NC-A is derived from two different carbon precursors, as discussed below. Comparably,

C and N atoms are evenly distributed in the carbon matrix of NC-A, with an N/C ratio of 3.8 wt.% (Figure 2i). This result indicates that N doping in the NC-A was preserved, albeit the exposure of p-MCEFs@M-PF to KOH caused the exfoliation of nanographitic π-stacks in the NC-A (Figure S8a). As anticipated, the NC-A sample exhibited a drastic increase in its S_{BET} (2191 $cm^2 g^{-1}$) but a decrease in its average pore diameter (2.6 nm), as contrasted with those of NC-U (Figure 2j and S6c). This should be attributed to the synergistic effects from the improved microporosity by KOH etching and the removal of p-MCEFs in p-MCEFs@M-PF by KOH activation, the latter of which was further confirmed by the absence of the mass-loss peak of p-MCEFs at about 350 °C in the TGA measurement of NC-A (Figure S5b). Therefore, the p-MCEFs in p-MCEFs@M-PF indeed play the role of pore-generating agents. As a control, we also prepared M-PF resin microspheres in the absence of p-MCEFs. The corresponding NC microspheres showed a low S_{BET}, no matter whether they were activated by KOH (MF-A) or not (MF-U) (Figure S6d, S9 and S10). Notably, this unique 3D structure of NC-A is expected to be an ideal design for ORR electrocatalysts due to the following advantages: 1) the 3D bi-continuous networks can facilitate electron transfer; 2) the hierarchically porous morphology can provide low-resistant diffusion channels for O_2 and electrolyte and thus ensure fast mass exchanges during the ORR process; 3) the well-distributed N element and high S_{BET} offer a high probability for the active sites exposure. All these favorable features could contribute to high rates of oxygen reduction.

To evaluate the effect of structure on the ORR catalytic activity, cyclic voltammetry (CV) tests (Figure S11a) were firstly performed on these as-prepared NC and the referenced Pt/C catalysts (E-TEK, 20%). In Ar environment, the CV curves of all metal-free samples were featureless, but their areas were highly correlated to the S_{BET} of the samples, suggesting a structure-amplified capacitor and electrode/electrolyte interface (Table S1). In O_2-saturated electrolytes, the CV peak potential (E_{peak}) positively shifted with increasing S_{BET} of the samples. Among them, the NC-A sample exhibited the best ORR activity with a well-defined E_{peak} at −0.168 V (Figure 3a). Similar trends were also observed in rotating-disk electrode (RDE) tests of the samples (Figure 3b). The higher the S_{BET} was, the more positive was the half-wave potential ($E_{1/2}$) and the higher was the limiting current density (J_L) the samples exhibited. As a result, the NC-A sample showed a nearly equal ORR activity to that of Pt/C catalysts in terms of their close $E_{1/2}$ (−0.133 and −0.128 V for NC-A and Pt/C, respectively) and J_L (4.54 and 4.66 mA cm^{-2} for NC-A and Pt/C, respectively). To our knowledge, this ORR-catalytic activity of NC-A is amongst the highest reported activities of metal-free NC catalysts.

Since these samples are similar in their N doping contents (Figure S9), it can be concluded that high S_{BET} indeed contributes to exposure of ORR catalytic sites. This is supported by the fact that the NC-A sample, despite a lower mass loading on the RDE, still exhibited a more positive $E_{1/2}$ than other samples (NC-U, MF-U and MF-A) (Figure 3b). To assess the unique structural advantages of NC-A, we further analyzed the Tafel curves of the NC-A sample with different mass loading on the RDE (Figure 3c and S12). In the low overpotential region (> −0.1 V), the NC-A sample had a Tafel slope between 41.67 and 46.28 mV dec^{-1}, slightly smaller than that of Pt/C catalysts (56.5 mV dec^{-1}), revealing a high surface ORR rate.[13] At a higher overpotential (<-0.15 V), Tafel slopes of the NC-A sample increased and lay between 73.21 and 82.31 mV dec^{-1}. Such a result implies a decreased ORR rate resulting from an increased exposure of certain low active sites; that is, S_{BET}-promoted exposure of catalytic sites is independent of their activity. However, in stark contrast to the sharp increase of the Tafel slopes of some reported metal-free NC catalysts in the high overpotential region,[2d] Tafel slopes of NC-A showed a relatively stable and smaller value, rigidly proving its excellent mass-transfer property. Taken together, these data unambiguously suggest that the unique structural advantages of NC-A help to enhance both the exposure and the utilization of ORR active sites.

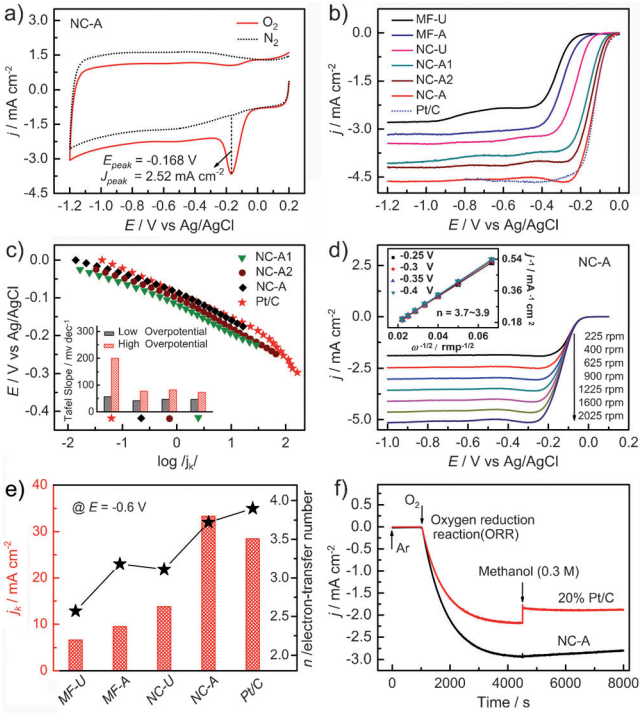

Figure 3. a) CV curves of NC-A in Ar- and O_2-saturated 0.1 M KOH aqueous solution. The scan rate was 50 mV s^{-1}. b) Linear-sweep voltammetry (LSV) curves of various samples in O_2-saturated 0.1 M KOH electrolyte at a scan rate of 10 mV s^{-1} and a rotation rate of 1600 rpm. c) Tafel plots derived from Figure 3b in the low-current region. Inset: The corresponding slope values of Tafel plots in both low and high overpotential regions. d) LSV curves of NC-A at different rotating rates. Inset: The corresponding Kouteckey–Levich plots at different potentials. e) Summary of the kinetic limiting current density (j_K) and the electron-transfer number (n) on the basis of the RDE data on various samples (at −0.6 V). f) Chronoamperometric response of NC-A and Pt/C at −0.25 V in Ar-saturated 0.1 M KOH solution followed by introduction of O_2 and methanol. Metal-free catalyst loadings are 0.128 $mg_{cat} cm^{-2}$; Pt/C loading is 0.102 $mg_{cat} cm^{-2}$ (E-TEK, 20%). NC-A1 (0.038 $mg_{cat} cm^{-2}$) and NC-A2 (0.077 $mg_{cat} cm^{-2}$) catalysts represent NC-A samples with a lower mass loading.

For further insight into the ORR kinetics, the kinetic parameters including kinetic current density (J_K) and electron transfer number (n) were analyzed on the basis of the RDE measurements at various rotating speeds and the Koutecky–Levich (K–L) equations (Figure 3d, S13, and S14). As shown in Figure 3e, the MF-U and NC-U samples typically exhibited a mixed two- and four-electron pathway for ORR (MF-U, $n=2.57$ and NC-U, $n=3.11$, at -0.6 V) and a low J_K (6.57-13.8 mA cm^{-2}), similar to those reported for N-doped M-PF derived carbons.[14] Although the NC-U sample showed a higher J_K than MF-A, the MF-A sample had a slightly larger n almost over the entire potential range (Figure S15a). This finding implies that activation of M-PF resins with KOH, rather than high S_{BET}, can partly promote the ORR through a four-electron pathway on the resultant NC catalysts. Remarkably, the NC-A sample exhibited a nearly four-electron process for ORR ($n=3.72$, at -0.6 V), with a high J_K of 33.24 mA cm^{-2}. This value is about 3.5 times larger than that of MF-A ($J_K=9.5$ mA cm^{-2}) and superior to that of the Pt/C catalysts ($J_K=28.46$ mA cm^{-2}), further suggesting the unique structural advantages of NC-A. Significantly, the NC-A sample also showed a better tolerance to methanol crossover effect and better long-term durability than commercial Pt/C (Figure 3f, S15b and S16). Both factors render NC-A a promising cathode catalyst for direct methanol fuel cells.

To elucidate the nature of catalytic sites in the as-prepared samples, we first examined their electrical conductivity by electrochemical impedance spectroscopy (EIS), as high electrical conductivity is a prime requirement for ORR catalysts. As shown in Figure 4a, the NC-A and MF-A samples exhibited an improved electrical conductivity compared to the NC-U and MF-U samples, respectively (see details in Figure S18), indicating that KOH activation enhances the electrical conductivity of M-PF derived carbons. This finding was further confirmed by the C1s XPS spectra of the MF-A and NC-A samples (Figure 4b, S19, S21 and Table S2), in which an improved degree of graphitization is deduced from the increase in the proportion of sp^2-C (284.5 eV)[15] and the decrease in the proportion of methylene bridge groups (284.0 eV).[16] Evidently, the NC-A sample showed the best electrical conductivity, partly explaining its high ORR activity. Interestingly, the NC-U sample exhibited a slightly higher electrical conductivity than MF-A, because of the larger electrode/electrolyte interface of NC-U. This result, in combination with the larger n of MF-A, implies that the nature of catalytic sites is not susceptible to the electrical conductivity of samples.

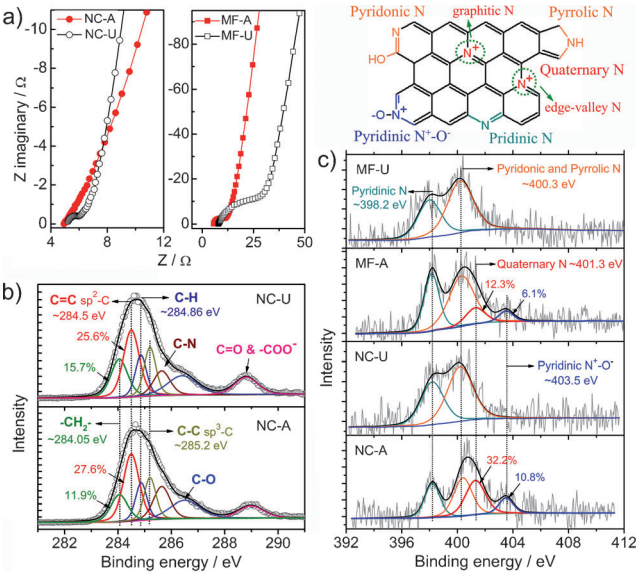

Figure 4. a) Nyquist plots, and b) high-resolution C1s and c) N1s XPS spectra of the as-prepared samples.

At this point, it is pertinent to investigate the chemical state of nitrogen in the samples by XPS analysis and to correlate the type of NDs with ORR activity (Figure 4c). The fine N1s XPS peak of MF-U and NC-U only pointed to the presence of two major NDs by their binding energies: pyridinic N (398.2 eV) and pyrrolic and pyridonic N (400.3 eV).[3b] Considering the small n of NC-U and MF-U, it is inferred that pyrrolic and pyridinic N were low effective ORR catalytic sites. This conclusion seems to contradict a previous report that pyridinic N species on the edge of N-doped graphene are very important for ORR.[6a] In our case, preferential exposure of edge graphitic planes, like in the case of two-dimensional graphene, is not expected to take place in the as-prepared samples.[8b]

Therefore, our conclusion is rational—that is, the catalytic efficiency of NDs in ORR highly depends on their degree of exposure on the carbon matrix. In sharp contrast, the N1s XPS peak of NC-A and MF-A consisted of two new components arising from the GNs (401.3 eV) and pyridinic N$^+$-O$^-$ (403.5 eV).[3b] Similar events were also observed in the NC-A sample at lower annealing temperature (Figure S20b). Such results appear to indicate that another vital effect of KOH activation was the fusion of nanographitic carbon platelets on which edge NDs became entrapped within a carbon lattice (to form GNs), similar to the effect of CO_2 activation.[17] Given that KOH activation mainly proceeded on the surface of M-PF resins, the GNs and pyridinic N$^+$-O$^-$ species should be sufficiently exposed on the resulting NC-A and MF-A samples. Considering the relatively larger n of NC-A and MF-A, as well as the inert nature of pyridinic N$^+$-O$^-$ species, we conclude that GNs catalyzes ORR through a four-electron pathway, in agreement with theoretical calculations.[4c,d] To our knowledge, this provides the first evaluation of ORR catalytic nature of GNs exposed directly on the surface of metal-free NC.

Recognition of the structural advantages of the NC-A sample has encouraged us to explore the formation mechanism of its 3D hierarchically porous framework (see details in Figure S23). In our hydrothermal conditions, two reactions should occur simultaneously (Figure 1): 1) the cellulose esters in the p-MCEF template dissolved and permeated the PDA coating, and then underwent hydrolysis, dehydration and carbonization;[18] 2) phenol was adsorbed on the adherent PDA coatings and in situ polymerized to M-PF resin in the presence of melamine and hexamethylenetetramine. It is reasonable to assume that the precursors have interpenetrated during these two reactions, thus offering one explan-

ation for the observed pore-generating ability of p-MCEFs. On this basis, it can be inferred that the sponge-like carbon films in the TEM images of NC-A were derived from the partially carbonized celluloses, while the carbon nanoparticles should stem from the M-PF resins, as supported by the differences in their Raman spectra (Figure S8).

In summary, we have developed a new and facile synthesis of 3D hierarchically porous NC materials by using p-MCEFs as both 3D macroporous templates and endogenous pore-generating agents, with the assistance of KOH activation. The as-prepared NC-A sample shows a super-high surface area ($2191\ cm^2 g^{-1}$) and hierarchical micro-, meso-, and macroporosity, thus enabling sufficient exposure and improved accessibility of ORR-catalytic sites. Our electrochemical tests in combination with XPS analysis prove that the outstanding ORR-catalytic activity of NC-A is derived from the GNs exposed on the surface layers, thereby experimentally disclosing the catalytic nature of GNs, which is of great importance for the design and development of advanced metal-free ORR catalysts. Considering the adherent availability of PDA on a variety of materials,[11] it is easy to envisage that this template-assisted approach can be also extended to the preparation of various nanostructured NC materials with expected capabilities for various applications, such as catalysis, supercapacitors, sensors, and metal–air batteries.

Received: April 15, 2014
Revised: May 27, 2014
Published online: July 10, 2014

Keywords: electrocatalysis · fuel cells · graphitic-N species · hierarchically porous structure · oxygen reduction

[1] a) M. K. Debe, *Nature* **2012**, *486*, 43; b) G. Wu, K. L. More, C. M. Johnston, P. Zelenay, *Science* **2011**, *332*, 443; c) Y. Liang, Y. Li, H. Wang, J. Zhou, J. Wang, T. Regier, H. Dai, *Nat. Mater.* **2011**, *10*, 780; d) S. Guo, S. Zhang, L. Wu, S. Sun, *Angew. Chem.* **2012**, *124*, 11940; *Angew. Chem. Int. Ed.* **2012**, *51*, 11770; e) F. Jaouen, E. Proietti, M. Lefevre, R. Chenitz, J. P. Dodelet, G. Wu, H. T. Chung, C. M. Johnston, P. Zelenay, *Energy Environ. Sci.* **2011**, *4*, 114.

[2] a) K. Gong, F. Du, Z. Xia, M. Durstock, L. Dai, *Science* **2009**, *323*, 760; b) B. Winther-Jensen, O. Winther-Jensen, M. Forsyth, D. R. MacFarlane, *Science* **2008**, *321*, 671; c) K. Ai, Y. Liu, C. Ruan, L. Lu, G. Lu, *Adv. Mater.* **2013**, *25*, 998; d) J. Liang, Y. Zheng, J. Chen, J. Liu, D. Hulicova-Jurcakova, M. Jaroniec, S. Z. Qiao, *Angew. Chem.* **2012**, *124*, 3958; *Angew. Chem. Int. Ed.* **2012**, *51*, 3892; e) I. Y. Jeon, H. J. Choi, S. M. Jung, J. M. Seo, M. J. Kim, L. Dai, J. B. Baek, *J. Am. Chem. Soc.* **2013**, *135*, 1386; f) D. Wang, D. S. Su, *Energy Environ. Sci.* **2014**, *7*, 576.

[3] a) L. Lai, J. Potts, D. Zhan, L. Wang, C. K. Poh, C. Tang, H. Gong, Z. Shen, J. Lin, R. Ruoff, *Energy Environ. Sci.* **2012**, *5*, 7936; b) T. Sharifi, G. Hu, X. Jia, T. Wagberg, *ACS Nano* **2012**, *6*, 8904; c) H. Niwa, K. Horiba, Y. Harada, M. Oshima, T. Ikeda, K. Terakura, J. i. Ozaki, S. Miyata, *J. Power Sources* **2009**, *187*, 93; d) H. Kim, K. Lee, S. I. Woo, Y. Jung, *Phys. Chem. Chem. Phys.* **2011**, *13*, 17505; e) R. Liu, D. Wu, X. Feng, K. Müllen, *Angew. Chem.* **2010**, *122*, 2619; *Angew. Chem. Int. Ed.* **2010**, *49*, 2565; f) R. Silva, D. Voiry, M. Chhowalla, T. Asefa, *J. Am. Chem. Soc.* **2013**, *135*, 7823.

[4] a) Y. Zhao, L. Yang, S. Chen, X. Wang, Y. Ma, Q. Wu, Y. Jiang, W. Qian, Z. Hu, *J. Am. Chem. Soc.* **2013**, *135*, 1201; b) F. Gao, G. L. Zhao, S. Yang, J. J. Spivey, *J. Am. Chem. Soc.* **2013**, *135*, 3315; c) R. A. Sidik, A. B. Anderson, N. P. Subramanian, S. P. Kumaraguru, B. N. Popov, *J. Phys. Chem. B* **2006**, *110*, 1787; d) T. Ikeda, M. Boero, S. F. Huang, K. Terakura, M. Oshima, J. i. Ozaki, *J. Phys. Chem. C* **2008**, *112*, 14706; e) D. Deng, X. Pan, L. Yu, Y. Cui, Y. Jiang, J. Qi, W. X. Li, Q. Fu, X. Ma, Q. Xue, G. Sun, X. Bao, *Chem. Mater.* **2011**, *23*, 1188.

[5] a) R. Arrigo, M. Havecker, S. Wrabetz, R. Blume, M. Lerch, J. McGregor, E. P. Parrott, J. A. Zeitler, L. F. Gladden, A. Knop-Gericke, R. Schlogl, D. S. Su, *J. Am. Chem. Soc.* **2010**, *132*, 9616; b) T. Sharifi, F. Nitze, H. R. Barzegar, C. W. Tai, M. Mazurkiewicz, A. Malolepszy, L. Stobinski, T. Wågberg, *Carbon* **2012**, *50*, 3535.

[6] a) W. Ding, Z. Wei, S. Chen, X. Qi, T. Yang, J. Hu, D. Wang, L. J. Wan, S. F. Alvi, L. Li, *Angew. Chem.* **2013**, *125*, 11971; *Angew. Chem. Int. Ed.* **2013**, *52*, 11755; b) S. Yang, X. Feng, X. Wang, K. Mullen, *Angew. Chem.* **2011**, *123*, 5451; *Angew. Chem. Int. Ed.* **2011**, *50*, 5339; c) X. H. Li, S. Kurasch, U. Kaiser, M. Antonietti, *Angew. Chem.* **2012**, *124*, 9827; *Angew. Chem. Int. Ed.* **2012**, *51*, 9689.

[7] D. Yu, Q. Zhang, L. Dai, *J. Am. Chem. Soc.* **2010**, *132*, 15127.

[8] a) E. J. Biddinger, U. S. Ozkan, *J. Phys. Chem. C* **2010**, *114*, 15306; b) P. H. Matter, L. Zhang, U. S. Ozkan, *J. Catal.* **2006**, *239*, 83.

[9] a) L. Wang, A. Ambrosi, M. Pumera, *Angew. Chem.* **2013**, *125*, 14063; *Angew. Chem. Int. Ed.* **2013**, *52*, 13818; b) W. Li, J. Wu, D. C. Higgins, J. Y. Choi, Z. Chen, *ACS Catal.* **2012**, *2*, 2761; c) J. S. Lee, G. S. Park, S. T. Kim, M. Liu, J. Cho, *Angew. Chem.* **2013**, *125*, 1060; *Angew. Chem. Int. Ed.* **2013**, *52*, 1026; d) Y. Li, W. Zhou, H. Wang, L. Xie, Y. Liang, F. Wei, J. C. Idrobo, S. J. Pennycook, H. Dai, *Nat. Nanotechnol.* **2012**, *7*, 394.

[10] a) J. Liang, X. Du, C. Gibson, X. W. Du, S. Z. Qiao, *Adv. Mater.* **2013**, *25*, 6226; b) D. W. Wang, F. Li, M. Liu, G. Q. Lu, H. M. Cheng, *Angew. Chem.* **2008**, *120*, 379; *Angew. Chem. Int. Ed.* **2008**, *47*, 373; c) G. S. Chai, I. S. Shin, J. S. Yu, *Adv. Mater.* **2004**, *16*, 2057.

[11] a) H. Lee, S. M. Dellatore, W. M. Miller, P. B. Messersmith, *Science* **2007**, *318*, 426; b) Y. Liu, K. Ai, L. Lu, *Chem. Rev.* **2014**, *114*, 5057.

[12] Y. Zhu, S. Murali, M. D. Stoller, K. J. Ganesh, W. Cai, P. J. Ferreira, A. Pirkle, R. M. Wallace, K. A. Cychosz, M. Thommes, D. Su, E. A. Stach, R. S. Ruoff, *Science* **2011**, *332*, 1537.

[13] a) M. T. de Groot, M. Merkx, A. H. Wonders, M. T. M. Koper, *J. Am. Chem. Soc.* **2005**, *127*, 7579; b) C. Coutanceau, M. J. Croissant, T. Napporn, C. Lamy, *Electrochim. Acta* **2000**, *46*, 579; c) D. B. Sepa, M. V. Vojnovic, A. Damjanovic, *Electrochim. Acta* **1986**, *31*, 91.

[14] Y. Sun, C. Li, G. Shi, *J. Mater. Chem.* **2012**, *22*, 12810.

[15] a) H. J. Shin, K. K. Kim, A. Benayad, S. M. Yoon, H. K. Park, I.-S. Jung, M. H. Jin, H. K. Jeong, J. M. Kim, J. Y. Choi, Y. H. Lee, *Adv. Funct. Mater.* **2009**, *19*, 1987; b) W. He, L. Lu, *Adv. Funct. Mater.* **2012**, *22*, 2542.

[16] S. Wang, X. Jing, Y. Wang, J. Si, *Polym. Adv. Technol.* **2014**, *25*, 152.

[17] M. Zhong, E. K. Kim, J. P. McGann, S. E. Chun, J. F. Whitacre, M. Jaroniec, K. Matyjaszewski, T. Kowalewski, *J. Am. Chem. Soc.* **2012**, *134*, 14846.

[18] X. Sun, Y. Li, *Angew. Chem.* **2004**, *116*, 607; *Angew. Chem. Int. Ed.* **2004**, *43*, 597.

